Method for Automatic Slippage Detection With Tactile Sensors Embedded in Prosthetic Hands

Rocco A. Romeo, Clemente Lauretti, *Member, IEEE*, Cosimo Gentile, Eugenio Guglielmelli, *Senior Member, IEEE*, and Loredana Zollo, *Senior Member, IEEE*

***Abstract*—Tactile sensing is fundamental for the human hand to achieve high dexterity. Most prosthetic hands are still devoid of tactile sensors, implying that the user cannot perceive external stimulation nor react in a fine manner. As a consequence, unforeseen events, e.g., slippage, are difficult to manage. This article proposes an algorithm to perform slippage detection with tactile sensors integrated into prosthetic hands. The algorithm is based on the filtering of the tactile sensor output; rectification and envelope follow the filtering. A binary signal, relating to slippage, is finally computed. An electrical circuit has been designed and built to elaborate the tactile signals. These have been embedded in a bioinspired fingertip mounted on a prosthetic hand, which has been interfaced with a robotic arm to assess the algorithm capability to identify slippage. Eight different surfaces have been employed, while three sliding velocities have been tested with a random interaction force between the fingertip and the test surfaces. Finally, experiments in a closed-loop configuration have been conducted to demonstrate the algorithm effectiveness in dynamic manipulation. Results proved the adequacy of the algorithm in terms of slippage detection and short latency between onset of slippage, actual detection and hand reaction.**

***Index Terms*—Algorithm, filter, fingertip, prosthesis, robot, sensor, slippage, tactile.**

I. Introduction

DESPITE the considerable progress in the design of prosthetic hands, the lack of tactile sensorization still represents a main concern. The human hand can actively control grasped objects of various shape and size, regulating force levels with very fast reaction times (around 0.1-0.2 s [1]). Such a performance is possible thanks to the thousands of tactile mechanoreceptors placed in the human skin, with a maximum concentration on the fingertip [2]. Conversely, prosthetic hands do not include tactile sensors in the majority of applications. There is no lack of adequate technology for the construction of effective tactile sensing elements; several reports [3], [4], attest to the enormous effort and progress achieved throughout the last decades. Instead, limitations are still significant when the tactile information has to be integrated in the control of the robotic hands. The current state of the art does not yet offer reliable algorithms and elaboration techniques which can be used on a large-scale perspective.

One of the crucial properties that characterize the human tactile system is the capability to react to unforeseen events, e.g., to slippage phenomena. The prevention of slippage events would add a strong contribution to the artificial sense of touch, allowing the introduction of tactile perception into the design of commercial robots. Although many approaches have been proposed, there is no consensus on an effective solution, resulting in a variegate scenario. We try to summarize it in the following:

1) Friction cone: It requires the measurement of both normal and tangential forces; the ratio of the tangential component to the normal one gives the friction coefficient. This must stay within the so-called friction cone in order to guarantee grasp stability. Three-axis force sensors [5] or even six-axis force/torque (F/T) sensors [6] are commonly used to pursue this approach.
2) Frequency analysis: By transforming the tactile sensor output in the frequency domain, hidden information about slippage might be retrieved. A gold standard is certainly the Fast Fourier Transform (FFT) [7], as well as the Short-Time Fourier Transform (STFT) [8], which avoids the loss of temporal resolution typical of the FFT. Signal power might also be adopted [9], or even the Discrete Wavelet Transform (DWT) [10]. Stationary Wavelet Transform (SWT) has also been employed very recently [11].
3) Piezoelectricity: Material like lead zirconium titanate (PZT) and polydimethylsiloxane (PDMS), when rubbed on a generic surface, produce voltages oscillating at high frequency. This characteristic confers to piezoelectric sensors suitability for slippage identification. Example of PDMS- [12] and PZT-based [13] sensors can be found in prosthetics as well.

Friction coefficient estimation often implies the use of multi-axial force sensors [14]; this is economically inconvenient, as multiaxial sensors are often more expensive than monoaxial ones. Moreover, the Coulomb model is inaccurate

Manuscript received October 24, 2020; revised January 5, 2021; accepted February 7, 2021. Date of publication February 18, 2021; date of current version May 20, 2021. This article was recommended for publication by Associate Editor M. Ortiz-Catalan and Editor P. Dario upon evaluation of the reviewers' comments. This work was supported in part by the Horizon2020 Research and Innovation Programme under Grant 899822 (SOMA Project), and in part by the INAIL Prosthetic Center with the WiFiMyo-Hand (CUP: E59E19001460005) Project. *(Corresponding author: Rocco A. Romeo.)*

Rocco A. Romeo was with CREO Lab, Università Campus Bio-Medico di Roma, 00128 Rome, Italy. He is now with Istituto Italiano di Tecnologia, iCub Tech Facility, 16163 Genoa, Italy (e-mail: rocco.romeo@iit.it).

Clemente Lauretti, Cosimo Gentile, Eugenio Guglielmelli, and Loredana Zollo are with the Research Unit of Biomedical Robotics and Biomicrosystems, Università Campus Bio-Medico di Roma, 00128 Rome, Italy (e-mail: c.lauretti@unicampus.it; c.gentile@unicampus.it; e.guglielmelli@unicampus.it; l.zollo@unicampus.it).

Digital Object Identifier 10.1109/TMRB.2021.3060032

for soft and very soft surfaces [15]. Piezoelectric sensors are commonly inadequate for static load estimation, requiring an additional sensor for force measurement. Their performance is also affected by temperature [16]. Frequency and time-frequency transformations always carry a certain computational burden; the same applies to learning algorithms that may be implemented, e.g., through neural networks (NN). In particular, NN usually need more sensors to generate a precise output, as in [17] where fingertips with six strain gages each were mounted on a robotic hand. The learning phase included data from a camera as well. In a more recent work [18], slip predictors were learned with data collected from a multi-channel fingertip. Learning paradigms, such as support vector machines and random forest classifiers, were implemented to perform slip prediction. Despite results showed good accuracy in both grip stabilization and slip prediction, the proposed learning approach required huge dataset from the fingertip, long time for training and eventually slower real-time execution. Large quantity of data were also required in [19], where slip was predicted basing on an Hidden Markov Model. It was trained with signals acquired by means of six-axis F/T sensors, several strain gages and PVDF sensing units.

In this article, we present an algorithm [20] for slippage detection and its hardware implementation. The algorithm needs only monoaxial data, which might be an uncalibrated voltage signal from a single tactile sensor (relating, e.g., to the normal force). The algorithm does not require tangential forces, though the algorithm might be applied on them when available. Hence, the algorithm can work with generic tactile sensors regardless the number of axes. The main operations composing the algorithm regard the filtering of the tactile signal and the computation of the envelope of the filtered signal. A definite ON-OFF signal is achieved by means of a thresholding procedure; said signal can be integrated in the closed-loop control of robotic hand prosthesis, as recently illustrated in [21] where a precedent version of the algorithm has been evaluated. Here, we propose an electrical circuit ad-hoc designed to execute the algorithm operations, thus notably reducing the computational time. Indeed, only the binary ON-OFF signal is created (online) via software during the real-time acquisition of the circuit output. Therefore, the algorithm is simple and fast, and guarantees the proper identification of slippage phenomena with tactile sensors.

To prove its reliability, experiments have been performed on a robotic setup composed of a robotic hand prosthesis interfaced to a robotic arm. Some purposely designed fingertips, featuring a piezoresistive tactile sensor, have been fabricated and mounted on the prosthetic hand. The algorithm has been tested in three different configurations: 1) sliding finger (SF), i.e., the robot moved the hand making the sensorized fingertip slide on the test surface; 2) sliding surface (SS), i.e., the hand grasped an object and the robot induced its slippage; 3) real manipulation (RM), i.e., the hand grasped an object, the robot induced its slippage and the hand was programmed to react avoiding the slippage. In the first configuration, six flat surfaces made of different materials, three of which with roughness a priori known, were used. In the second configuration, two non-flat objects were grasped by the hand and the robot caused their movement. Three sliding velocities have been tested; instead, force has been randomly applied by the robotic system on the surfaces to demonstrate independence from the exerted force. Five trials per each velocity have been carried out, leading to a total of 120 experiments for the first 2 configurations. In the third configuration, a set of four objects, two flat and two non-flat, were grasped by the hand. As the robot perturbed the grasp, the hand strengthened it to prevent the slippage in a closed-loop fashion. Each grasp test was repeated three times per object, achieving 12 more tests. In this final configuration, only one velocity was tested.

The main contribution of the present paper can be summarized in this way: 1) to deliver an effective slip-detection algorithm for prosthetics applications; 2) to provide a general hardware implementation of the algorithm, which is faster than its software version [22] and allows for prompt reaction in real manipulation; 3) to evidence the reliability of the algorithm on a much broader set of experimental conditions than in [22]. Importantly, the implementation proposed in this article was employed in an in-vivo experimentation on an amputee subject [23]. Nonetheless, the method is a valuable candidate for implementation on robotic hands and end-effectors, being simple, quick and able to work with whatever tactile sensor that provides a signal relating to the applied force. Other scenarios such as, e.g., surgical robotics, field robotics and rescue robotics could benefit from the application of a similar method.

The paper is structured as follows: Section II gives a brief overview of the human physiology inherent to the slippage perception, and of the proposed algorithm. Section III explains the implementation of the algorithm and describes the setup. Section IV illustrates and discusses the experimental results; finally, Section V refers conclusion and future work.

II. Slippage Detection Through Filters: Method Overview and Related Work

Slippage can be predicted thanks to the presence of vibrations. This comes from a physiological evidence; it is well known that vibrations activate Meissner's corpuscles (FA I) and Pacinian ones (FA II) of the human skin. The first have small receptive field and are sensitive to frequencies below 50 Hz, while the second have larger receptive field and precept the frequency of vibrations up to 500 Hz. FA I are supposed to be involved in the spontaneous reflex that controls the grip adjustment, e.g., when an object is slipping off [24]. FA II resonate when vibrations occur between the fingers and the gripped object. This condition often verifies when the object is starting to move with respect to the skin or vice versa. Interestingly, the nerve ending of FA II receptors is surrounded by a fluid-filled cavity and by an outer capsule composed of lamellar cells. These act as a mechanical filter, which inhibits low frequencies and relay to the axon only higher frequencies [24].

Likewise, mechanical stimuli enabling artificial tactile sensors might be filtered in order to obtain a useful slip signal. The idea of applying filters to tactile signals is relatively recent. Useful bandwidths have been identified depending on the employed sensor technology and on packaging, which

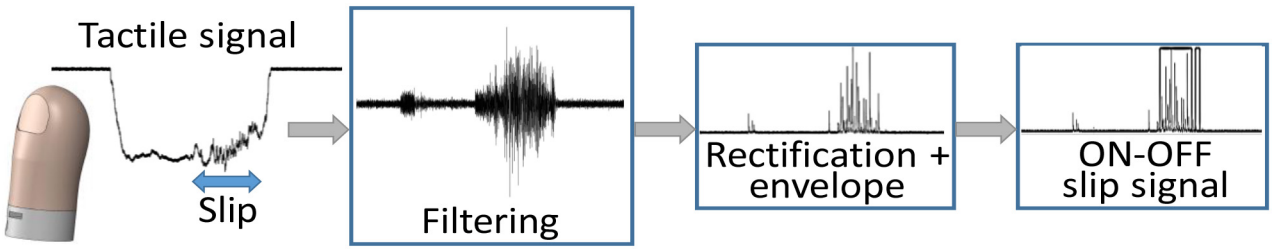

Fig. 1. Block diagram of the algorithm. The raw voltage signal has been collected from the bioinspired fingertip (see Section III-B) acting as the tactile sensing element of the robotic platform. After filtering the tactile signal, this has been rectified and enveloped. A binary ON-OFF signal relating to the presence of slip has been finally generated.

affect the sensor output. Resistive [25], capacitive [26], hydroacoustic [27] and optical sensors [28] have been adopted in both robotic and prosthetic applications. However, little attention has been paid to the analysis of the delay between detected slippage and actual onset. In [25] a cascade of seven digital band-pass filters was experimented so as to isolate a specific frequency interval; a further low-pass (LP) filter was added to reduce noise above the bandpass. Diversely, [26] illustrates how to high-pass (HP) filter the tactile signals from a sensor array so as to mimic the FA I behavior. Notwithstanding the quality of these woks, they do not provide details on the slip detection promptness of the proposed approaches. Authors of [27] analyze time response of two methods, one based on derivative and one on BP filtering of a force signal estimated from the electrodes voltage of a biomimetic fingertip. The downside was that delay was compared with the movement onset provided by an IMU attached to the slipping object but no detail on how fast was the IMU was given. The same applies to [28] where optical sensors were attached to a prosthetic hand. HP filtering was also employed in [29] to perform preliminary elaboration of tactile data; these were collected from the piezoresistive sensors of a robotic hand. The detection delay was not examined in this work at all.

We propose instead a detailed analysis of the algorithm performance concerning such a delay. Furthermore, the outcome of the algorithm is a digital ON-OFF signal which no longer needs to be processed. A monoaxial force information is enough; no tangential forces nor learning paradigms are necessary to implement the algorithm. We already showed the potentiality of digital filters for the slippage detection [22]. Here, we propose a hardware implementation to minimize latency in computation. Moreover, we extended the algorithm validity on a wider set of surfaces and sliding velocities, applying random forces instead of predefined ones (as detailed in the Introduction).

The algorithm block scheme is depicted in Fig. 1. The main steps can be summarized as follows: 1) filtering network 2) half-wave rectification 3) envelope 4) binary ON-OFF computation. Although the last operation is performed via software, the absence of digital filters allows to greatly reduce the delay introduced by their intrinsic causality.

The first step regards the extraction of the vibrations from the tactile signal and can be done with at least one analog filter. It serves to penalize all the undesired frequencies from the tactile sensor output. The uncalibrated voltage output might be the input of the network when available, as there is no need to transform such a voltage into a force value. Voltage variations yielded by the slippage phenomenon can be extracted by means of the filter network, thus performing the force estimation in parallel with the slippage identification. The filter network gives a bipolar signal which can be rectified to elide negative (or positive) variations. For this purpose, in the second step one or more diodes have to be adopted downstream of the filter network. Half-wave or full-wave rectification is possible, though half-wave one is preferable as it requires a minor number of physical components. The envelope, at the next step, smooths the rectified signal so as to clear too fast variations and helps the subsequent thresholding mechanism work better. In a circuit, this operation is performable through a first-order LP filter in series with the rectification diodes. Finally, the binary ON-OFF signal is computed on predefined windows of enveloped signal thanks to the aforementioned thresholding, which works on a threshold empirically chosen.

III. Materials and Methods

A. Slippage Detection Algorithm: Implementation

The algorithm overview has been presented in Section II. Here, its physical implementation will be detailed. A Printed Circuit Board (PCB) has been designed; the PCB hosted the analog circuit that processed the tactile signal before the acquisition by the DAQ board.

Filter network. The piezoresistive sensor mounted inside the fingertip (see Section III-B) behaves as a varying electrical resistance. When no load is applied onto it, this resistance is an open circuit. Instead, a load of 0.2 N to above shorts the traces of the two layers thanks to the presence of carbon ink. Hence, the resistance starts decreasing; a simple circuit (not shown here) composed of a Wheatstone bridge and of an instrumentation amplifier converts the value of the resistance into a voltage. This is the input for the filter network. A high order is desirable so as to obtain a fast roll-off, penalizing frequencies outside the useful bandwidth of the tactile signals. A third order can be sufficient as it guarantees a slope of -60 Decibel per decade (dB/dec) on a double logarithmic scale. To implement it, two filters with different structure and order have been cascaded. Both filters have been mounted in non-inverting configuration.

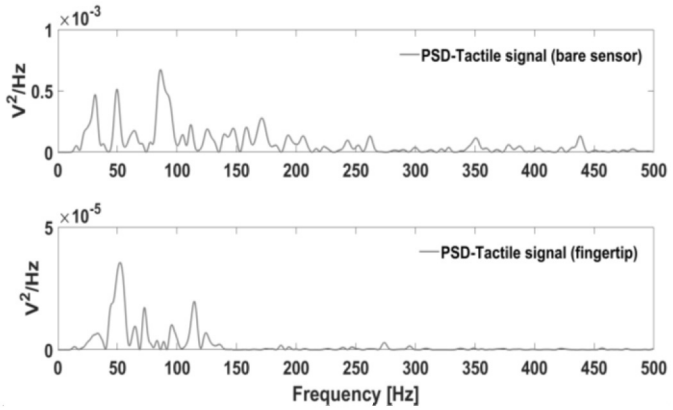

Fig. 2. PSD of the piezoresistive tactile signal. Sensor with no cover (top) and embedded in the fingertip (bottom). Frequency content extends above 200 Hz when the sensor is used bare, whereas the silicon cover attenuates vibrations resulting into lower frequencies.

The chosen modality for the filters has been HP. Such a modality actually acts as a BP filter between a given cut-off frequency f_c and $f_s/2$, being f_s=2kHz the sampling frequency. This way, a reduced number of electrical components can be used to design the network. In this concern, the use of stopband filters of previous work [22] has been avoided, rendering the circuit layout simpler. Moreover, another significant novelty w.r.t. [22] resides in the identification of a general bandwidth, valid even when the test surface has no ridges and when its roughness is unknown. To this end, the spectra of a number of collected signals have been observed. Fig. 2 shows the power spectrum density (PSD) of signal portions as wide as 512 ms. One signal relates to a sliding movement carried out with the bare sensor, whereas the other relates to a trial performed with the sensor integrated in the biomorphic fingertip. From the plots, one may find meaningful components at different frequencies; the fingertip spectrum of course misses some of them, as the silicon cover dampens higher frequencies. That is, it provides a LP action. Indeed, frequency content manifested above 100 Hz very rarely. On the other hand, with the bare sensor frequencies up to 200 Hz appear predominant, with minor (but not negligible) components above 200 Hz. To properly set the filter network, its cut-off frequency f_c has been set at 67 Hz. This choice derived from the analysis of the contact events, which can be often misunderstood for slip phenomena and whose frequency content is located below 30 Hz. The chosen f_c permits to include in the network bandwidth the higher components that have been observed up to 100 Hz for the fingertip signals, as well as the components up to above 200 Hz typical of the bare sensor slippage.

The first filter was a first-order HP filter, designed with a closed-loop gain G=66.7 in linear scale (around 36.5 dB). Its transfer function $H_1(\omega)$ in the frequency domain is given by:

$$H_1(\omega) = \frac{G}{\iota\omega + \frac{1}{R_1 C_1}}\iota\omega, \tag{1}$$

where $G = H_1(\infty)$ is expressed as:

$$G = 1 + R_5/R_4. \tag{2}$$

The Bode diagram of the filter transfer function is plotted in Fig. 4, whereas the filter schematic is available in Fig. 3, which shows the whole circuit schematic. A quite high gain G has been set to amplify the filtered signal; to this aim, resistors R_5 and R_4 were 100 kΩ and 1.5 kΩ, respectively. The second filter was a second-order HP filter, in the Sallen-Key topology. This filter has been created with a unitary gain, letting G control the overall gain of the network and facilitating the computation of the transfer filter function $H_2(\omega)$. Hence, it can be written as follows:

$$H_2(\omega) = \frac{-\omega^2}{-\omega^2 + \frac{(C_2+C_3)}{R_3 C_2 C_3}\iota\omega + \frac{1}{R_2 R_3 C_2 C_3}}. \tag{3}$$

By selecting the filter capacitors such that C_2=C_3=C, (3) simplifies to:

$$H_2(\omega) = \frac{-\omega^2}{-\omega^2 + \frac{2}{R_3 C}\iota\omega + \frac{1}{R_2 R_3 C^2}}. \tag{4}$$

At this point, the correct value of the resistors must be identified. Said value depends also on the type of filter that one wants to construct. In the present case, the Butterworth filter has been determined to be the most suitable for the application, thanks to the maximum flatness of its passband which does not feature undesired ripples (like, e.g., Chebyshev filters). That is, all the frequencies in the passband are equally amplified, resulting in the absence of signal distortion. Besides, its phase has good linearity. The value of the resistors R_1, R_2 and R_3 can be found through the following relations:

$$R_1 = \frac{1}{a_1 C \omega_c} \sim 2.4\ k\Omega, \tag{5}$$

$$R_2 = \frac{a_2}{2 b_2 C \omega_c} \sim 1.2\ k\Omega, \tag{6}$$

$$R_3 = \frac{2}{a_2 C \omega_c} \sim 4.7\ k\Omega. \tag{7}$$

These values represent the closest available ones, normally with 1-2% tolerance. The coefficients a_1, a_2 and b_2 are given by the filter theory and may be retrieved from literature [30]. In (5)-(7), C_1=C=1 μF and a_1=a_2=b_2=1.

Fig. 4 illustrates the Bode diagram of the second filter transfer function and of the entire network. The circuit has been dimensioned to feature a quality factor Q=1. This led to a maximally flat response in the passband (Fig. 4), which is typical of Butterworth filters. Given the filter configuration (HP) and that C_2=C_3=C, Q depends solely on the value of R_2 and R_3 according to the following formula:

$$Q = \sqrt{R_3/4R_2}. \tag{8}$$

Higher quality factors would allow a better storage of the energy in the circuit, though flatness would be lost above the cut-off frequency. In the current implementation of the algorithm, all the frequencies in the passband have been amplified in the same way. Further, it is worth noticing that the chosen operational amplifier (TL082B by Texas Instruments, Inc.) had a good gain-bandwidth (GBW) product, i.e., 3 MHz. This ensured the correct functioning of the amplifier even if the value of G has been set quite high. The GBW characteristic is depicted in Fig. 4 together with the transfer

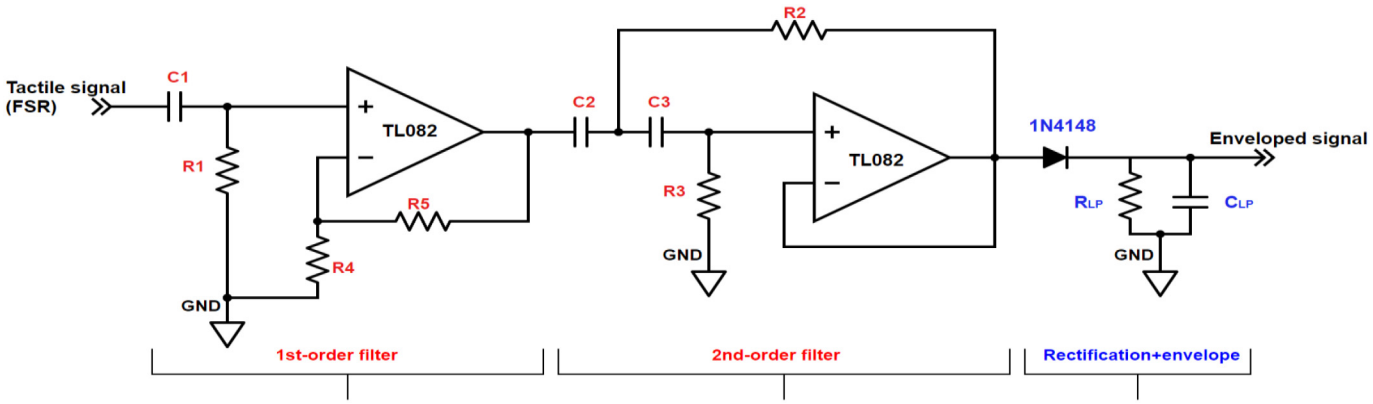

Fig. 3. Schematic diagram of the circuit. The 1^{st}- and 2^{nd}-order filters extract the slippage content from the tactile signal collected by the sensor inside the fingertip. Then the diode and the LP filter rectify and envelop the filtered signal, which is collected and thresholded so as to compute an ON-OFF slip signal.

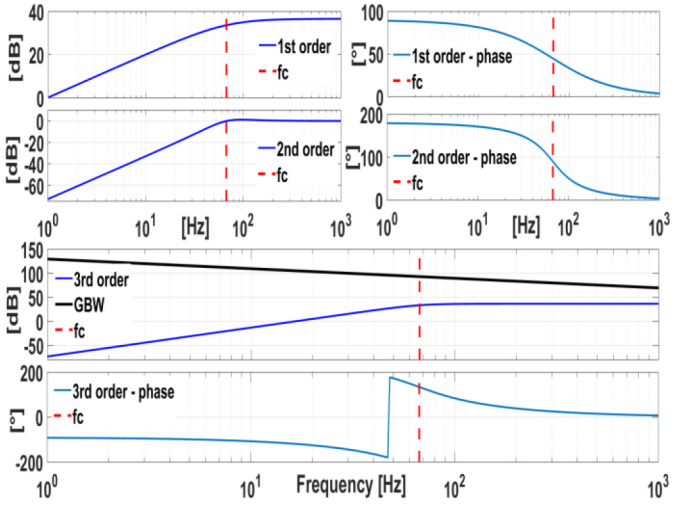

Fig. 4. Filter response at each stage. 2^{nd}-order filter has steeper transition between passband and stopband than 1^{st}-order one. Amplitude loss is clearly more prominent in the 2-nd order filter. The 3^{rd}-order function stands below the GBW of the chosen amplifier. Phase trend is coherent with the number of poles and zeros of the transfer function at each stage.

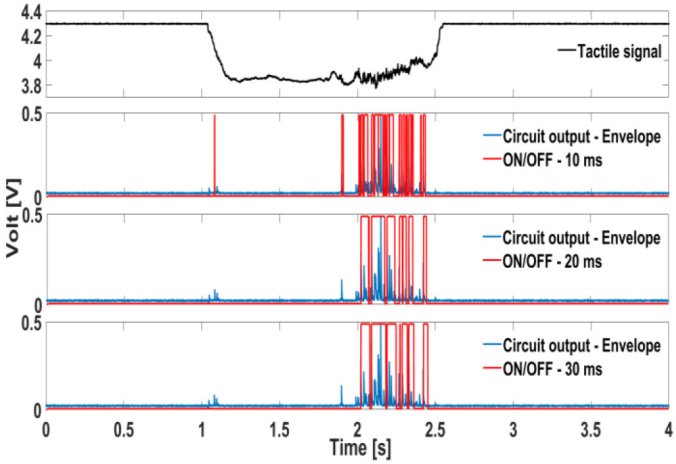

Fig. 5. Algorithm output for different window lengths L. A too little L increases the possibility to detect false positives, e.g., when the fingertip contacts a surface. This happens (after 1 s) with an L of 10 ms. A longer L helps avoid this issue. Acceptable values range from 20 ms to above, though L must be lower than 100 ms to ensure coherency with human physiology.

function of the network. The final transfer function $H_c(\omega)$ of the network is the product of the transfer functions of the two filters $H_1(\omega)$ and $H_2(\omega)$, and can be written in this manner:

$$H_c(\omega) = \frac{G\ \iota\omega}{\iota\omega + \omega_c} \cdot \frac{-\omega^2}{-\omega^2 + \frac{\iota\omega\omega_c}{Q} + {\omega_c}^2}, \tag{9}$$

in which w_c=$2\pi f_c$ is the cut-off angular frequency and its link to the circuit components is denoted by:

$$\omega_c = \frac{1}{R_1 C} = \frac{1}{\sqrt{R_2 R_3}C}, \tag{10}$$

whence $R_1 = \sqrt{R_2 R_3}$. This relation may be easily verified considering the values calculated in (5), (6) and (7), confirming the correctness of the component selection for the network.

Rectification and envelope. To rectify the filtered signal, the simplest way is to place a diode downstream of the filter network. In this manner, only one polarization, either positive or negative (depending on the diode orientation), proceeds towards the circuit output achieving a half-wave rectification. A similar operation differs from the absolute value computation in that the signal is devoid of the negative (in our case) peaks, which will not be converted into positive ones. The half-wave rectification allows using fewer components with respect to (w.r.t.) the full-wave one, which requires four diodes instead of one. The loss of one polarization is acceptable, as the half-wave rectified signal is sufficiently powerful for the next algorithm steps.

Downstream of the diode, a LP filter performed the envelope of the rectified signal. This stage elided the useless fluctuations characterizing the filtered and rectified signal, yielding instead a smoother waveform. The result of this operation resembles the computation of the Root Mean Square (RMS). The transfer function $H_{LP}(\omega)$ of the LP filter is defined by the equation below:

$$H_{LP}(\omega) = \frac{1/C_{LP}}{\iota\omega + \omega_{LP}}, \tag{11}$$

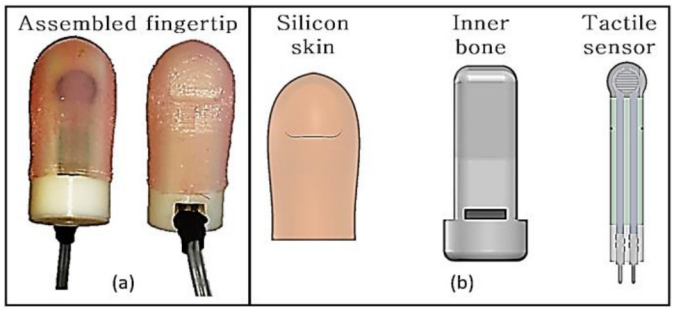

Fig. 6. Bioinspired fingertip. Assembled prototype (front/rear). The sensor body has been lodged along the bone and ran out through its posterior hole (a). Exploded CAD view with silicon cover and inner bone to which the tactile sensor has been attached (b).

where $\omega_{LP} = (R_{LP}C_{LP})^{-1}$. The filter cut-off frequency $f_{LP}=\omega_{LP}/2\pi$ was 36.17 Hz. Thus, a suitable choice was: $R_{LP}=2\ k\Omega$ and $C_{LP}=2.2\mu F$. The cut-off frequency f_{LP} could be fixed at lower values, achieving a higher time constant $\tau_{LP} = R_{LP}C_{LP}$ and longer discharge time of the capacitor C_{LP}. Yet f_{LP} has been set to a value which avoided the risk to lose some signal meaningful content.

Binary slip signal. The final step towards obtaining a definite slip signal foresaw the computation of a binary ON-OFF waveform. To carry out this task, the enveloped signal has been analyzed through a temporal window of predefined length. When the mean amplitude of the samples was higher than an empirically determined threshold, the ON level was yielded. Vice versa, the slip signal was kept at the OFF level. The window extension has been carefully identified in order to elide false positives. A too short window might result into an activation of the binary signal during, e.g., the contact phase, when the fingertip touched the test surface. Thus, a minimum length $L=60$ (i.e., 30 ms) has been heuristically found. Fig. 5 shows the algorithm output for different values of L. During each trial, the ON-OFF signal has been computed in real time through a LabVIEW program, updating the window with a new sample at each program iteration with a resolution of $1/f_s$, i.e., 0.5 ms. The window W_i can be mathematically defined at each iteration i as:

$$W_i = \left[E_{i-L+1}, E_{i-L+2}, \ldots E_i\right] \tag{12}$$

meaning that the included L samples went from the *(i-L+1)-th* sample of the enveloped signal E to the current *i-th* sample.

B. Bioinspired Fingertip

To perform the experiments, a specific setup has been created. Such a setup included a robotic arm and a robotic hand prosthesis (see Section III-C). The robotic prosthesis has been endowed with a tactile sensor to measure the force level during the experimental trials. To this end, a new fingertip has been designed. Each prosthetic finger has two phalanxes: the proximal phalanx (the closest to the palm) is made of aluminum while the distal phalanx (i.e., the fingertip) is made of rubber. The new fingertip replaced the latter in the index finger. The piezoresistive tactile sensor (Fig. 6b) has been a Force Sensing Resistor (FSR, model FSR400 by Interlink Electronics, Inc.); FSRs are widely used in prosthetic experiments and are commonly small, flexible, with linear response. An FSR basically behaves as an electrical resistance, as stated earlier. A pressure applied on its sensitive area causes a diminishment of the resistance value. A simple circuit (briefly described in Section III-A) converted the electrical resistance variation into a voltage. A calibration procedure [21] has been carried out in the force range 0-8 N to derive a mathematical function that links the voltage output of the circuit to the actual normal force. Hysteresis of the employed FSR sensor has been empirically evaluated in [31] to ensure that it does not exceed 10%.

We adopted the CAD software SolidWorks for the fingertip design, which has subsequently been fabricated by means of a high-resolution 3-D printer. The fingertip (Fig. 6a) has been conceived with a size slightly larger than FSR 400. Internally, a solid structure (bone) has been mounted with the sensor and covered with a prosthetic silicon encapsulation (40 shore A) obtained through an ad-hoc designed mold. In this way, the sensor has been totally covered with prosthetic silicon, which is very resistant and rather soft at the same time, allowing the fingertip to convey the applied force onto the sensor sensitive area. A hole has been designed at the base of the bone, permitting the cables soldered to the sensor tabs to run within its structure and to be placed on the back of the fingertip. Therefore, no obstruction from cables was present between the anterior face of the fingertip and the test surface. Fig. 6b shows an exploded view of the designed fingertip. CAD images of the silicon skin, of the bone and of the FSR sensor are shown separately. Following the same criteria, another version of the fingertip has been projected with larger size so as to host the FSR402 FSR model. This has been used in the RM configuration to allow for a greater contact area during the closed-loop manipulation experiments.

C. Experimental Setup and Protocol

The proposed algorithm for slippage detection has been experimentally validated on an arm-hand robotic system composed of the KUKA Light Weight Robot 4+ (LWR 4+) and the IH2 Azzurra hand (Fig. 7). The LWR 4+ is a 7-DoF (Degree of Freedom) robotic arm with position and torque sensors at its joints. The IH2 robotic hand (by Prensilia Ltd.) has been attached to the LWR 4+ wrist in order to act as the hand of the robotic system. It is a 11-DoF, 5-finger robotic hand with weight and size similar to the human ones. Depending on the experiment type, the hand fingers have been endowed with the previously shown fingertip embedding the FSR that measured the normal interaction force between the finger and the test surface.

During the experimental session, three configurations have been adopted: 1) sliding finger 2); sliding surface; 3) sliding surface with closed-loop control. In the first one (SF), the LWR 4+ robot has been moved so as to make the index fingertip of the prosthetic hand slip on the test surfaces at different velocities. During the slippage, the surfaces were attached to a fixed support by means of an adhesive material. The robotic manipulator has been piloted through a PID

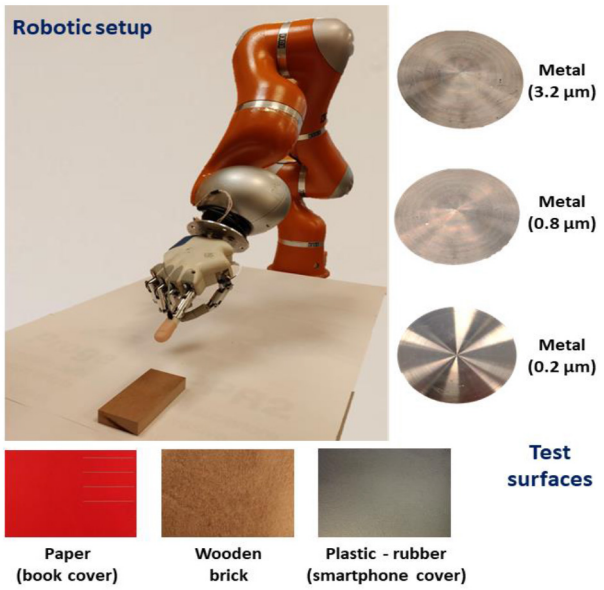

Fig. 7. Experimental setup and test surfaces. The anthropomorphic, robotic hand (IH2) is interfaced to the LWR 4+ robot, and is endowed with the bioinspired sensorized fingertip.

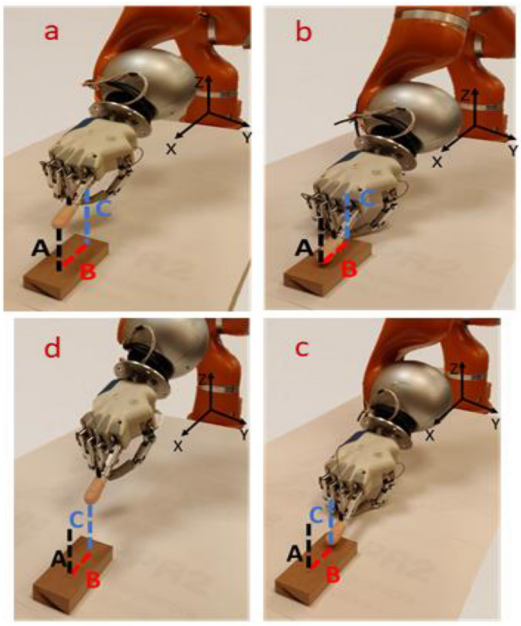

Fig. 8. Illustration of the robot end effector motion during the experiments. Path A, B and C are the tip-surface approach, tip-surface sliding and the tip-surface distancing, respectively. The robotic arm-hand system approached the test surface (a) and came into contact with it (b). Then the fingertip was slid over the surface (c) and finally released (d).

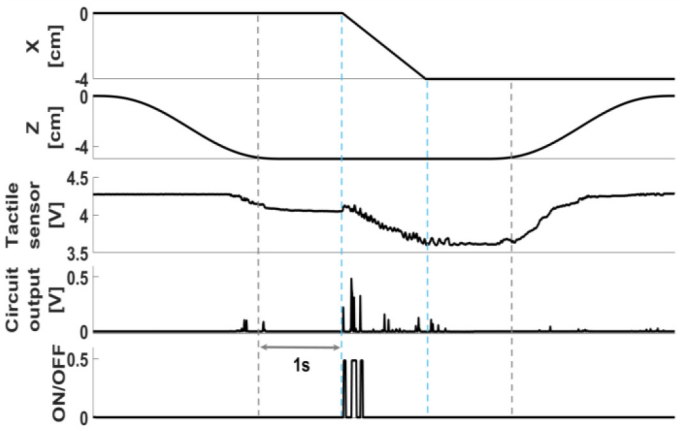

Fig. 9. Typical trial with relevant signals, SF configuration. The robot movement along Z-Axis, i.e., the normal direction, brought the fingertip into contact with the surface. As the contact began (grey line on the left), a slight force was recorded and then one second was waited before initiating the actual slip (between the light blue lines) along the X-Axis. In this phase, vibrations in the signals are evident. The slip lasted one second (trial velocity: 4 cm/s) and then another second lapsed prior to lifting the fingertip from the surface (grey line on the right). During the slip, the circuit output (enveloped signal) evidently grew and the application of a thresholding to it yielded an ON-OFF signal relating to the actual slip. The same applies to SS configuration, except that the fingertip is already in contact with the test surface as the test starts.

velocity control used to slide the fingertip on the surfaces. In particular, the algorithm has been tested at three different sliding velocities, i.e., 4cm/s, 6cm/s and 8 cm/s, with six surfaces (Fig. 7). Three of these surfaces were metallic and their roughness was known, i.e., 0.2 μm (smooth), 0.8 μm (medium) and 3.2 μm (gross), while the remaining three were common textures with unknown roughness, i.e., wood, paper (book cover) and plastic (smartphone cover). All the tested surfaces had frictional properties typical of Activities of Daily Life (ADLs). Five trials have been executed at each velocity level, achieving 15 trials per surface and 90 experiments in total.

As shown in Fig. 8, the robot motion during each trial could be divided into 3 phases: tip-surface approach and contact (path A); tip-surface sliding (Path B); tip-surface distancing (path C). For the tip-surface approach and tip-surface distancing phase the robot end-effector orientation has been kept constant.

Fig. 9 illustrates the signals characterizing a generic SF trial. During the tip-surface approach, the robot end-effector has been moved linearly for 2 centimeters, along the negative Z-Axis from the starting position showed in Fig. 8 (Path A). The position along the other directions, i.e., X and Y, as well as the robot end-effector orientation, were constant. The target position along the Z-Axis has been randomly varied within 4-6 cm at each trial. This condition guaranteed that the trials were performed with a random fingertip-surface interaction force, so as to prove independence of the algorithm output from said force. The resulting interaction force recorded during the SF experiments ranged from 0.2 N to 2 N.

During the tip-surface sliding (between the dashed light blue lines), the robot end-effector has been moved 4 cm along the negative X-Axis and its motion has been planned through a trapezoidal velocity profile. The peak velocity has been set at 4cm/s, 6cm/s or 8 cm/s. In this case, the position along the other directions, i.e., Z and Y, as well as the robot end-effector orientation, were constant.

During the tip-surface distancing, the robot end-effector has finally been moved of 5 cm in 2 seconds along the positive Z-Axis. As for the tip-surface approach, the robot position along the other directions, i.e., X and Y, as well as the robot end-effector orientation, were again constant.

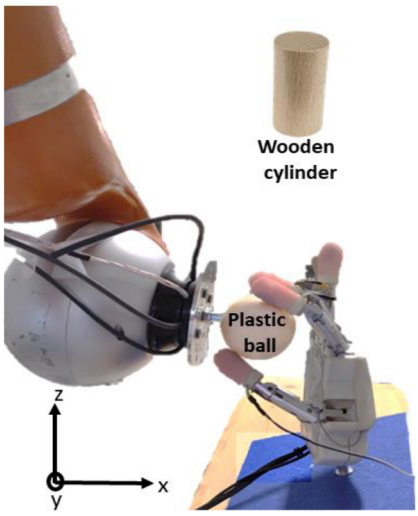

Fig. 10. Experimental setup and test surfaces for the SS configuration. In this case, the experimental protocol was simpler than SF: the robot, to which the object was attached through a metallic pin, has been pre-positioned such that the hand was able to grasp the object in a tri-digital fashion. Then, the robot moved the object along the X-Axis and provoked relative sliding with the hand fingers. The hand was mounted on a fixed support.

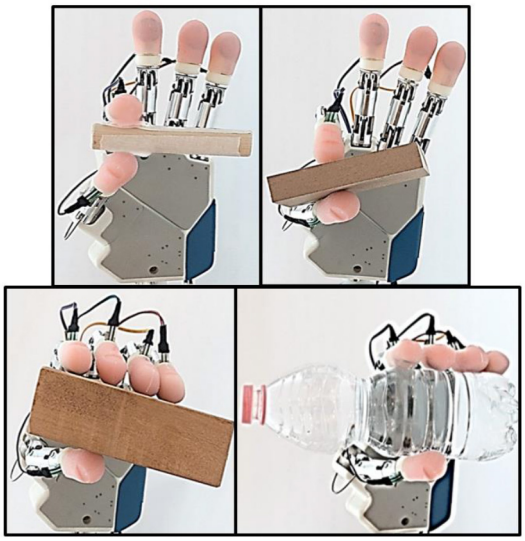

Fig. 11. RM grasps: pinch, cylinder (top left); pinch, small parallelepiped (top right); power, bottle (bottom right); power, parallelepiped (bottom left).

In all the trials, a time lapse of one second between each phase and the following one has been set. This can be viewed in Fig. 9: after the tip-surface contact (dashed grey line on the left), one second passed before slip commenced. When the slip was over, another second passed before the fingertip was released (dashed grey line on the right). In this manner, contact and release could be distinguished from the actual slippage.

In the second configuration (SS), the robot has been controlled in the same way as in the first. The protocol was the same as in the SF configuration expect that there was neither tip-surface approach nor tip-surface distancing. Indeed, in this configuration the object has been interfaced with the robot through a metallic pin as illustrated in Fig. 10. The robot has been pre-positioned so that the object could be placed among the prosthetic hand fingers, which were in turn pre-positioned to perform a tri-digital grasp. Only Path B was executed, along the positive X-Axis. Therefore, as the trial commenced, the hand was commanded to complete the tri-digital grasp and the robot moved the object to induce slippage. Even in this case, the robot end-effector motion has been planned through the same trapezoidal velocity profile as in SF configuration. Applied force by the robot has been again randomly generated, as well as the grip force exerted by the prosthetic hand during the tri-digital grasp. Two objects have been tested with same velocity levels as for SF configuration, achieving 30 trials. Recorded forces could be greater than 3 N in the SS trials.

In the third configuration (RM), experiments have been conducted as in the second one, though the hand could this time react reproducing a real-manipulation scenario. In fact, a control strategy [32] has been employed to actuate the prosthetic hand; such a strategy used the ON-OFF slippage information, as well as the measured force, to modify the position of the hand fingers. The thumb abduction/adduction (A/A) and the flexion/extension (F/E) of all the fingers but the little have been registered. Indeed, ring and little fingers of the IH2 hand are mechanically coupled and subject to the same movements. As a slippage event was detected, the hand automatically tightened the grasp. When the object was firmly grasped, the robot induced the slippage by hitting the grasped object (manually prepositioned) with the metallic pin of the SS configuration, which in this case has not been interfaced to the object itself. For each object, the grasp has been repeated three times at the same velocity (i.e., 8 cm/s), leading to 12 tests. Two grasp types have been selected: pinch and power. The power grasp has been set to last 1 second more than the pinch grasp. The prosthetic hand grasped 4 objects, namely: parallelepiped (255 g), bottle of water (500 g), parallelepiped (60 g), cylinder (20 g). The first two have been grasped with the power grasp, whereas for the last two it has been adopted the pinch grasp. All the objects were rigid and made of wood except for the bottle which was made of plastic and was therefore deformable. Roughness was unknown for all the four objects, as for typical daily-life objects. Note also that the for the RM configuration, the prosthetic hand was instrumented with five sensorized fingertips to collect force signals from all the fingers. Fig. 11 depicts the 4 RM grasps performed.

The data from the tactile sensor have been acquired at a frequency of 2 kHz through a DAQ device (NI 6002 by National Instruments, Inc.). The end-effector position along the tridimensional coordinate frame has been retrieved through application of direct kinematics on the joint angles; these have been measured by the robot encoders and sampled at 100 Hz. As each SF trial started, a trigger signal has been automatically sent from one analog output of the DAQ device to the robot control unit in order to synchronize acquisition of tactile and position data. As regards the SS trials, after the completion of the tri-digital grasp, a trigger signal has been sent to the robot as the FSR sensed a non-null force (i.e., the voltage started dropping). The same applied to pinch and power grasp in the RM configuration.

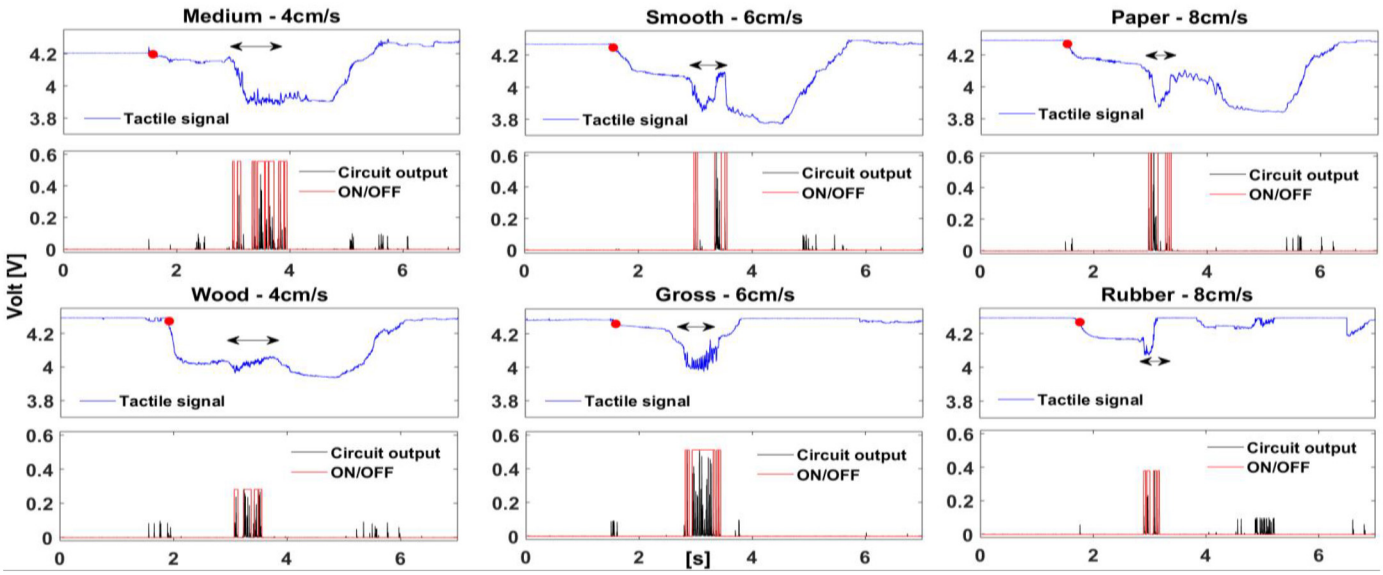

Fig. 12. Representation of a significant trial for each test surface, SF configuration. The algorithm output (ON-OFF) is shown for all the plots together with the enveloped signal (circuit output) and the original tactile signal. Two trials per each velocity are illustrated: the black double arrow covers the slippage, and the red dot indicates the tip-surface contact.

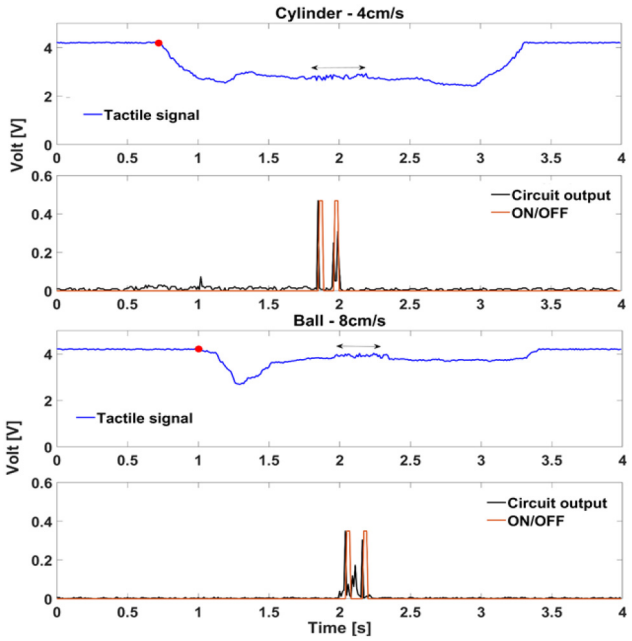

Fig. 13. Representation of a significant trial for each test surface, SS configuration.

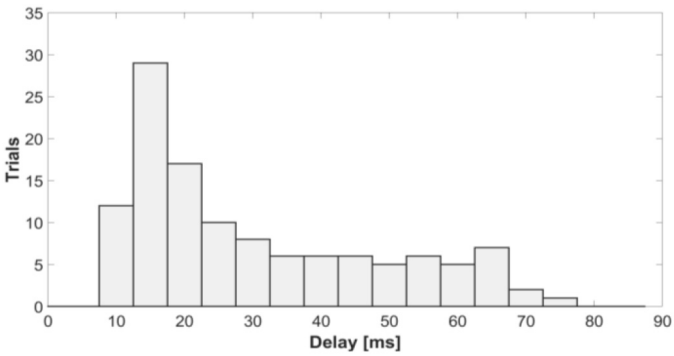

Fig. 14. Distribution of trials in delay intervals.

IV. Experimental Results

The performance of the proposed algorithm has been evaluated in terms of correct slippage identification and delay w.r.t. the slippage onset.

A. Algorithm Performance

We first proceed illustrating the results of the SF and SS configurations, in which the prosthetic hand could not react to the slippage.

Fig. 12 illustrates a representative trial relating to each tested surface of the SF configuration, covering all the sliding velocities. To show reliability regardless the applied force, the indentation force has not been directly controlled (as previously referred). Indeed, variable force can be noticed after the contact of the fingertip with the surfaces (red dot) and during the induced slippage (black double arrow). In the displayed trials, voltages (blue traces) ranging from 4.3 V to 4 V indicate up to 0.8 N as far as regards the contact phase, whereas during and after slippage, voltages can be as low as 3.85 V implying force level of maximum 1.3 N. The correct identification of slippage is denoted by the ON signal superimposed on the circuit output (enveloped signal). The ON corresponds to the portion of the force signal where vibrations attest the presence of slippage. From Fig. 12, one may observe how the slippage phenomenon, in some cases, provoked the loss of optimal fingertip contact. This resulted into a sudden diminishment of the recorded force (i.e., the voltage rises); nonetheless, even a very brief portion of signal carrying the slippage vibrations has been sufficient to detect the movement of the fingertip. In this case, a shorter duration of the ON phase is noticeable (see, e.g., the rubber trial).

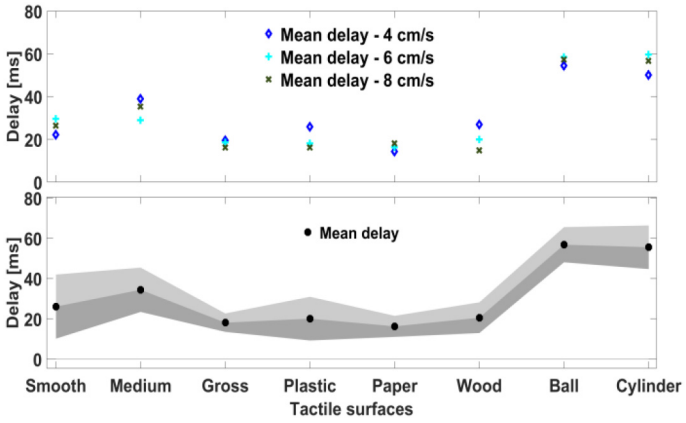

Fig. 15. Average delays. The top subplot displays all the tactile surfaces at each of the tested slippage velocity. The bottom subplot shows the overall average with standard deviation (grey areas) for all the surfaces.

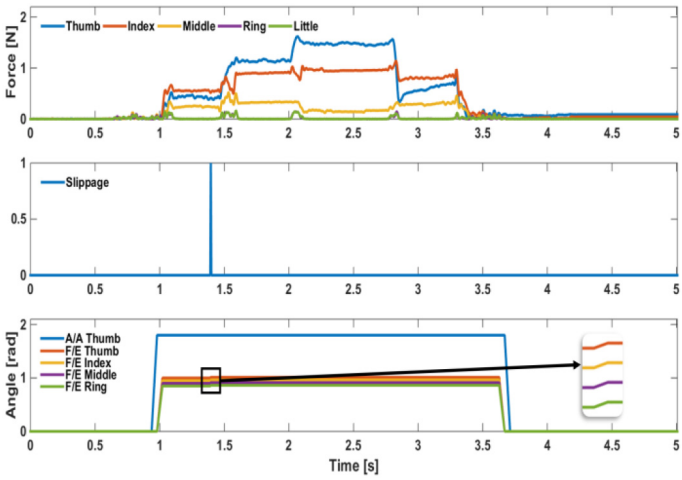

Fig. 16. Real manipulation of the parallelepiped, power grasp. The top subplot shows the force signals from all the hand fingers; the middle subplot shows the slippage ON-OFF signal; the bottom subplot shows the fingers position.

Another clear feature in Fig. 12 is the correlation of vibrations amplitude with the material. As it can be expected, a small roughness (e.g., the smooth surface, 0.2 μm) produced limited vibrations when compared to coarser materials such as surfaces with 0.8 μm and 3.2 μm roughness. The vibrations amplitude appears to grow proportionally to roughness. Wood seems to show more dense vibrations than paper and rubber even though its displayed trial had half velocity. Similarly, this is probably due to its higher roughness. Moreover, the amplitude of the enveloped signal (circuit output) related to the applied force, i.e., higher force corresponded to more power in the filtered signal, thus in the enveloped waveform.

Figure 13 displays a meaningful trial with the non-flat objects of the SS configuration. During these trials, voltage dropped to lower levels than in SF configuration, yielding forces even higher than 3 N. This descends from the tri-digital grasp performed by the prosthetic hand, which has been programmed with high gains to ensure stable grasp in the pre-slip phase. As the voltage started decreasing, one second passed before the robot moved: slip has been promptly detected even though the contact condition was not optimal and the applied force was little (e.g., in the ball trial). Roughness of both objects was unknown, however their surface was quite smooth, resulting in small vibrations that did not produce a continuous slip signal (as for the 0.2 μm surface of SF configuration).

The performance of the hardware implementation of the proposed algorithm has shown promising performance in the identification of slippage. Across the 120 trials, the slippage event has always been detected with rather low delays. Fig. 14 shows histograms indicating the occurrences of different delays. The histograms are centered at multiples of 5; a considerable concentration is evident in the 15-ms bin, which includes the trials with a delay between 12.5 ms and 17.5 ms. Remarkably, 69/120 trials (around 76.7%) showed a delay lower than 30 ms. These results indicate fast detection of slippage; this is of vital importance to provide the prosthetic system with the possibility to react in proper time (i.e., maximum 100 ms) to correct the grip force.

Fig. 15 displays the average delay measured on each surface per each sliding velocity tested (top subplot). The higher delay values characterize the trials on the smoothest surfaces, i.e., the ones with roughness equal to 0.2 μm and 0.8 μm, as well as the two objects of the SS configuration (which were also quite smooth). This finding suggests that the frictional properties of the surface have greater impact on the slippage detection than the sliding velocity. Indeed, the trend of the average delay across all the surfaces does not manifest significant difference from one velocity level to the other. This is confirmed by the overall mean value for each surface, where the aforementioned surfaces show the highest delay value. The standard deviation (shaded area) gives an idea of the variability in the measured delay: its maximum value has been around $\pm$15 ms (0.2 μm roughness). Nonetheless, its magnitude is acceptable as the mean value did never overcome 60 ms except for the two objects of SS configuration (see bottom subplot).

Finally, the results of the RM configuration are analyzed. 2 representative RM experiments are illustrated in Fig. 16 (parallelepiped, power grasp) and Fig. 17 (cylinder, pinch grasp). For these experiments, we show the calibrated force in place of the raw voltage as the hand control was based on the force feedback. In both figures, one can see that the thumb slippage onset is always followed by a variation of the fingers position due to the closed-loop action. The thumb A/A has been programmed to remain constant even after slippage, as its movement could lead to grasp instability. F/E of all the fingers changed to oppose the object slippage. In the power grasp, the slippage is followed by an increment in the force of all the fingers: this behavior was a consequence of the closed-loop force control. On the contrary, in the pinch grasp the contact force was already higher than the desired one, and the hand controller was not able to correct it immediately; when the slippage caused a diminishment in the applied forces, the controller could correctly adjust them avoiding slippage.

The pinch grasp that we show is significant also for the false positive detected at the contact. The hand control discarded it assuming that, when the forces are growing, slippage occurrence cannot happen. Out of 12 RM tests, we encountered two false positives: this one and another occurred during a test

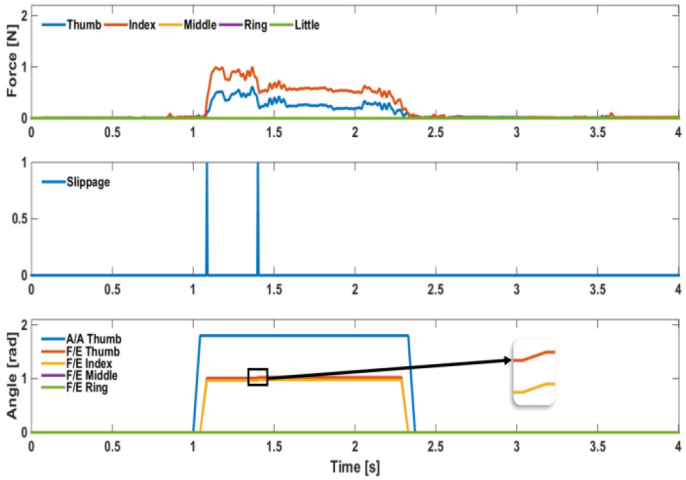

Fig. 17. Real manipulation of the cylinder, pinch grasp. The top subplot shows the force signals from all the hand fingers; the middle subplot shows the slippage ON-OFF signal; the bottom subplot shows the fingers position.

with the small parallelepiped. Hence, the slippage detection method resulted to be very robust. Bi-digital grasp appeared more likely to generate false positives and this was probably due to the small size of the objects, meaning higher grasp complexity. Nonetheless, no more false positives have been found even though the force waveforms fluctuated evidently (Fig. 17) due to limited contact area of the fingertips during the cylinder pinch grasp.

Besides, it is worth observing the mean reaction time of the hand after the integration of our slippage detection algorithm in the loop. Such a time is lower than 200 ms across all the 12 RM tests, and is in line with human response time for voluntary grip adjustment [1]. By allowing for very fast detection, our algorithm helped the hand accelerate its reaction preventing the grasped object from falling in 10 out of 12 dynamic tests. In the two failures, slippage was anyway detected with proper delay, though the object slipped off.

B. Comparison With Previous Works

Previous implementation of the present algorithm was detailed in [22] and resorted to digital filters. This allowed reaching rather low delays w.r.t. the slip onset though the average delay for each tested surface was in the range 36-48 ms. Moreover, the tested surfaces were only three and were ridged. Here we obtained a notable performance enhancement by replacing digital filters with analog ones, reducing the detection delay to less than 30 ms in most of cases. As also explained in the Introduction, here we performed experiments with more test surfaces and sliding velocities, and in different contact configurations. Further, we inserted the algorithm in closed-loop control strategies, achieving a prosthetic hand reaction time lower than 200 ms and a success rate of 83.33% (10/12).

Another significant comparison can be done with previously mentioned methods of [27]–[28]. Authors did grasping experiments with artificial hands endowed with tactile sensors and retrieved the time delays occurring between slip detection and slip onset. In [27] an IMU was attached to the grasped objects: authors could detect slip 35.7 $\pm$ 6 ms before the IMU in the best case. This gives an idea of how fast was their method if compared to the IMU, but does not clarify how fast such a method was overall. A similar argument might be valid against the method of [28] as well: the delays, always lower than 100 ms, were evaluated considering the IMU as a ground truth. In both studies, the grasping experiments were conducted with a human operator inducing the slip to the grasped objects (e.g., pouring water in a grasped cup). Differently, for this task we used a robot whose 3-D position was acquired in real time providing an objective reference. Moreover, the optical slip sensor of [28] cannot detect force, for which another sensor would be required. Our algorithm is based on a voltage output which can be easily transduced into a force signal. That is, both force and slip are detectable from a single waveform.

Finally, we present the results of another state-of-the-art method which started being employed early in slip identification, i.e., FFT. FFT is particularly suitable when the frequency content of a certain signal is to be studied. We used a 128-sample window, corresponding to a 64-ms temporal window (the same adopted in [7]). The slip was found when the FFT amplitude was greater than a threshold. Such an approach led to a true positive identification in less than 65% of cases. In the remaining ones, FFT presented meaningful spectra only after 100 ms the slip onset. A similar result is explainable by considering that the vibrations magnitude varies according to the test surface. When vibrations are weak, as it may happen in the normal force signal, frequencies relating to slip are hard to find with a simple spectrum. Tangential forces suits better the FFT application as they are characterized by more evident vibrations [7], [28]. Therefore, a well-designed filter network is more effective when the sole normal force is available.

Given the absence of multi-axial force components and of other sensors, we could not implement learning paradigms and compare with works such as [18]–[19]. However, according to the experimental comparison carried out in [33], the reaction time is shorter when using a filter-based approach rather than a learning-based one.

Notwithstanding the deep effort spent in this area, many researchers are still working to: 1) compare existing methods [27], [28], [33]; 2) figure out new slippage detection approaches featuring e.g., learning paradigms [17]–[18]. However, similar approaches commonly employ more sensor units, resulting in a certain degree of complexity. On the contrary, methods featuring the use of simple and low-cost tactile sensors would allow reducing such a complexity, thus favouring the ease of online implementation. Filters-based techniques, e.g., the one presented in this article, can use a monoaxial sensor to perform both slip detection and force estimation (as done in [21], [23]). Carrying out both operations with a single sensor leads to minimal encumbrance as well.

C. Current Limitations

The proposed method has two main limitations regarding the followings aspects:

1) Difference in mechanical response from one surface to the other might affect the filters behavior. Therefore,

even though in the present study we strived to conceive an implementation which is as general as possible, further investigation with more materials is reasonably required. For instance, we found that the detection delay seems higher on smooth surfaces, and this is allegedly due to their smaller friction.

2) When contact conditions are imperfect, such as in the case of small and/or instable contact area, the method performance deteriorates. To guarantee proper functioning, including false positives avoidance, the force signal (either calibrated or not) is expected to have a good quality. If this signal carries fluctuations due to instability during grasping, the result might be a false activation of the binary slip signal. Such an instability may be observed, e.g., in Fig. 17, relating to the pinch grasp of the small cylinder. The contact surface is indeed littler than in the other RM tasks.

V. Conclusion

In this article, we described a method for the automatic detection of slippage through a tactile sensor embedded in a prosthetic hand. The method consists of a network of analog filters and of a stage of rectification and envelope. The enveloped signal is then converted into an ON-OFF signal by means of a thresholding mechanism. The filter network extracts a meaningful slippage content from the tactile traces recorded by the tactile sensor. The following rectification and envelope modify the filtered signal in a such a way that the thresholding mechanism is easier to be applied. The method has been mainly implemented by means of a hardware, i.e., a PCB, which avoided the lag due to the use of digital filters as in [22]. The sole thresholding has been performed via software. Simple sensors measuring only the normal force component can be used, as no tangential forces are required.

An experimental setup has been created for the validation of the proposed method. The setup included a robotic arm-hand system. The hand has been endowed with bioinspired fingertips embedding FSR tactile sensors. The arm-hand system has been actuated in order to: 1) slide the fingertip onto six flat surfaces with different frictional properties 2) slide two objects with non-flat surface while being grasped by the prosthetic hand 3) perform real manipulation experiments featuring hand reaction. Three slippage velocities have been tested on each surface by imposing random normal forces, achieving an overall number of 120 trials. Results indicate a mean delay lower than 60 ms for all the surfaces in the first two configurations. Overall delay between onset of slippage and hand reaction has been lower than 200 ms, indicating the algorithm ability to successfully work within a state-of-the-art control strategy. Furthermore, the onset of slippage has been always correctly identified, regardless the slippage velocity and the normal force amplitude.

Future work will deal with the improvement of the circuit design. For instance, a voltage comparator might be added to generate the ON-OFF signal, replacing this way the use of software and performing the algorithm entirely via hardware. We also have to enhance the method performance w.r.t the limitations reported in Section IV-C; on smooth surfaces, the detection delay appears higher. Moreover, the performance on bi-digital grasp of small objects shall be ameliorated.

Finally, we also plan to carry out the RM tasks with higher force levels. In the present study, the employed controller [32] was set to generate low desired forces as the tested objects were rather light, i.e., max 500 g $\sim$ 5 N. Human manipulation tasks might involve forces up to 10 N [16] but we foresee to achieve even higher values to replicate tridigital and power grasps with heavy ($>$1000 g) objects.

References

[1] R. S. Johansson and G. Westling, "Signals in tactile afferents from the fingers eliciting adaptive motor responses during precision grip," *Exp. Brain Res.*, vol. 66, no. 1, pp. 141–154, 1987.

[2] R. S. Johansson and Å. B. Vallbo, "Tactile sensory coding in the glabrous skin of the human hand," *Trends Neurosci.*, vol. 6, pp. 27–32, Jan. 1983.

[3] M. Park, B.-G. Bok, J.-H. Ahn, and M.-S. Kim, "Recent Advances in Tactile Sensing Technology," *Micromachines*, vol. 9, no. 7, p. 321, 2018.

[4] C. Chi, X. Sun, N. Xue, T. Li, and C. Liu, "Recent progress in technologies for tactile sensors," *Sensors*, vol. 18, no. 4, p. 948, 2018.

[5] M. R. Tremblay and M. R. Cutkosky, "Estimating friction using incipient slip sensing during a manipulation task," in *Proc. IEEE Int. Conf. Robot. Autom.*, Atlanta, GA, USA, 1993, pp. 429–434.

[6] R. Bayrleithner and K. Komoriya, "Static friction coefficient determination by force sensing and its application," in *Proc. IEEE/RSJ/GI Int. Conf. Intell. Robots Syst. Adv. Robot. Syst. Real World (IROS)*, vol. 3. Munich, Germany, 1994, pp. 1639–1646.

[7] R. Fernandez, I. Payo, A. S. Vazquez, and J. Becedas, "Micro-vibration-based slip detection in tactile force sensors," *Sensors*, vol. 14, no. 1, pp. 709–730, 2014.

[8] D. Goger, N. Gorges, and H. Worn, "Tactile sensing for an anthropomorphic robotic hand: Hardware and signal processing," in *Proc. IEEE Int. Conf. Robot. Autom.*, Kobe, Japan, 2009, pp. 895–901.

[9] B. Heyneman and M. R. Cutkosky, "Slip classification for dynamic tactile array sensors," *Int. J. Robot. Res.*, vol. 35, no. 4, pp. 404–421, 2016.

[10] Y. Wang, K. Xi, and D. Mei, "Slip detection in prosthetic hand grasping by using the discrete wavelet transform analysis," in *Proc. IEEE Int. Conf. Adv. Intell. Mechatronics (AIM)*, Banff, AB, Canada, 2016, pp. 1485–1490.

[11] R. A. Romeo *et al.*, "Identification of slippage on naturalistic surfaces via wavelet transform of tactile signals," *IEEE Sensors J.*, vol. 19, no. 4, pp. 1260–1268, Feb. 2019.

[12] A. Mingrino, A. Bucci, R. Magni, and P. Dario, "Slippage control in hand prostheses by sensing grasping forces and sliding motion," in *Proc. IEEE/RSJ/GI Int. Conf. Intell. Robots Syst. Advan. Robot. Syst. Real World (IROS)*, vol. 3. Munich, Germany, 1994, pp. 1803–1809.

[13] D. P. J. Cotton, P. H. Chappell, A. Cranny, N. M. White, and S. P. Beeby, "A novel thick-film piezoelectric slip sensor for a prosthetic hand," *IEEE Sensors J.*, vol. 7, no. 5, pp. 752–761, May 2007.

[14] R. A. Romeo and L. Zollo, "Methods and sensors for slip detection in robotics: A survey," *IEEE Access*, vol. 8, pp. 73027–73050, 2020.

[15] R. D. Howe, I. Kao, and M. R. Cutkosky, "The sliding of robot fingers under combined torsion and shear loading," in *Proc. IEEE Int. Conf. Robot. Autom.*, Philadelphia, PA, USA, 1988, pp. 103–105.

[16] R. S. Dahiya, G. Metta, M. Valle, and G. Sandini, "Tactile sensing—From humans to humanoids," *IEEE Trans. Robot.*, vol. 26, no. 1, pp. 1–20, Feb. 2010.

[17] K. Hosoda, Y. Tada, and M. Asada, "Internal representation of slip for a soft finger with vision and tactile sensors," in *Proc. IEEE/RSJ Int. Conf. Intell. Robots Syst.*, vol. 1. Lausanne, Switzerland, 2002, pp. 111–115.

[18] F. Veiga, J. Peters, and T. Hermans, "Grip stabilization of novel objects using slip prediction," *IEEE Trans. Haptics*, vol. 11, no. 4, pp. 531–542, Oct./Dec. 2018.

[19] N. Jamali and C. Sammut, "Slip prediction using hidden Markov models: Multidimensional sensor data to symbolic temporal pattern learning," in *Proc. IEEE Int. Conf. Robot. Autom.*, Saint Paul, MN, USA, 2012, pp. 215–222.

[20] R. A. Romeo, L. Zollo, and E. Guglielmelli, "Method for detection of slippage with force sensors and apparatus thereof," Patent Appl. 102 016 000 105 302, Oct. 2016.

[21] R. Barone *et al.*, "Multilevel control of an anthropomorphic prosthetic hand for grasp and slip prevention," *Adv. Mech. Eng.*, vol. 8, no. 9, 2016, Art. no. 1687814016665082.

[22] R. A. Romeo, C. M. Oddo, M. C. Carrozza, E. Guglielmelli, and L. Zollo, "Slippage detection with piezoresistive tactile sensors," *Sensors*, vol. 17, no. 8, p. 1844, 2017.

[23] L. Zollo *et al.*, "Restoring tactile sensations via neural interfaces for real-time force-and-slippage closed-loop control of bionic hands," *Sci. Robot.*, vol. 4, no. 27, p. eaau9924, 2019.

[24] A. Zimmerman, L. Bai, and D. D. Ginty, "The gentle touch receptors of mammalian skin," *Science*, vol. 346, no. 6212, pp. 950–954, 2014.

[25] E. D. Engeberg and S. G. Meek, "Adaptive sliding mode control for prosthetic hands to simultaneously prevent slip and minimize deformation of grasped objects," *IEEE/ASME Trans. Mechatronics*, vol. 18, no. 1, pp. 376–385, Feb. 2013.

[26] J. M. Romano, K. Hsiao, G. Niemeyer, S. Chitta, and K. J. Kuchenbecker, "Human-inspired robotic grasp control with tactile sensing," *IEEE Trans. Robot.*, vol. 27, no. 6, pp. 1067–1079, Dec. 2011.

[27] Z. Su *et al.*, "Force estimation and slip detection/classification for grip control using a biomimetic tactile sensor," in *Proc. IEEE-RAS 15th Int. Conf. Humanoid Robots (Humanoids)*, Seoul, South Korea, 2015, pp. 297–303.

[28] A. Nakagawa-Silva, N. V. Thakor, J.-J. Cabibihan, and A. B. Soares, "A bio-inspired slip detection and reflex-like suppression method for robotic manipulators," *IEEE Sensors J.*, vol. 19, no. 4, pp. 12443–12453, Dec. 2019.

[29] M. Stachowsky, T. Hummel, M. Moussa, and H. A. Abdullah, "A slip detection and correction strategy for precision robot grasping," *IEEE/ASME Trans. Mechatronics*, vol. 21, no. 5, pp. 2214–2226, Oct. 2016.

[30] T. Kugelstadt, "Active filter design techniques," in *Op Amps for Everyone*, 3rd ed. Boston, MA, USA: Elsevier, 2009, pp. 365–438.

[31] R. A. Romeo *et al.*, "Development and preliminary testing of an instrumented object for force analysis during grasping," in *Proc. IEEE 37th Annu. Int. Conf. Eng. Med. Biol. Soc. (EMBC)*, Milan, Italy, 2015, pp. 6720–6723.

[32] F. Cordella *et al.*, "A force-and-slippage control strategy for a poliarticulated prosthetic hand," in *Proc. IEEE Int. Conf. Robot. Autom. (ICRA)*, Stockholm, Sweden, 2016, pp. 3524–3529.

[33] J. Reinecke, A. Dietrich, F. Schmidt, and M. Chalon, "Experimental comparison of slip detection strategies by tactile sensing with the BioTac®on the DLR hand arm system," in *Proc. IEEE Int. Conf. Robot. Autom. (ICRA)*, Hong Kong, 2014, pp. 2742–2748.